

Coordination-driven magnetic-to-nonmagnetic transition in manganese doped silicon clusters

V. Zamudio-Bayer,^{1,2,*} L. Leppert,^{3,†} K. Hirsch,^{1,2} A. Langenberg,^{1,2} J. Rittmann,^{1,2} M. Kossick,^{1,2} M. Vogel,^{1,2} R. Richter,² A. Terasaki,^{4,5} T. Möller,² B. v. Issendorff,⁶ S. Kümmel,³ and J. T. Lau^{1,‡}

¹*Institut für Methoden und Instrumentierung der Synchrotronstrahlung,
Helmholtz-Zentrum Berlin für Materialien und Energie GmbH,
Albert-Einstein-Straße 15, 12489 Berlin, Germany*

²*Institut für Optik und Atomare Physik, Technische Universität Berlin, Hardenbergstraße 36, 10623 Berlin, Germany*

³*Theoretische Physik IV, Universität Bayreuth, 95440 Bayreuth, Germany*

⁴*Cluster Research Laboratory, Toyota Technological Institute,
717-86 Futamata, Ichikawa, Chiba 272-0001, Japan*

⁵*Department of Chemistry, Kyushu University, 6-10-1 Hakozaki, Higashi-ku, Fukuoka 812-8581, Japan*

⁶*Fakultät für Physik, Universität Freiburg, Stefan-Meier-Straße 21, 79104 Freiburg, Germany*

(Dated: June 11, 2021)

The interaction of a single manganese impurity with silicon is analyzed in a combined experimental and theoretical study of the electronic, magnetic, and structural properties of manganese-doped silicon clusters. The structural transition from exohedral to endohedral doping coincides with a quenching of high-spin states. For all geometric structures investigated, we find a similar dependence of the magnetic moment on the manganese coordination number and nearest neighbor distance. This observation can be generalized to manganese point defects in bulk silicon, whose magnetic moments fall within the observed magnetic-to-nonmagnetic transition, and which therefore react very sensitively to changes in the local geometry. The results indicate that high spin states in manganese-doped silicon could be stabilized by an appropriate lattice expansion.

PACS numbers: 36.40.Cg, 75.50.Pp, 73.22.-f, 61.46.Bc

The interaction of a deliberately introduced impurity with a semiconductor material is one of the most fundamental problems of semiconductor physics. For magnetic impurities, an important question is the survival or quenching of the magnetic moment. From the pioneering studies of Ludwig and Woodbury [1] up to the present day, a wealth of experimental and theoretical studies have therefore been devoted to magnetic properties of transition metal doped semiconductors [2–6], semiconducting nanocrystals [7–9], and clusters [10–14]. A possible correlation between local magnetic moment and coordination number of the impurity has been noticed in theoretical work [6], but is challenging to investigate in bulk samples because of inhomogeneities, coalescence, or impurity band formation. These difficulties can be overcome by utilizing size-selected, singly-doped clusters as model systems where a transition metal atom occupies a well-defined position in the silicon host, without any interaction between impurities. Here, we study MnSi_n^+ by x-ray absorption and x-ray magnetic circular dichroism (XMCD) spectroscopy of size-selected free clusters [15–19] as a local and element-specific probe of electronic structure and magnetic properties. These experimental techniques are combined with non-empirical density functional theory (DFT) calculations. We find a clear dependence of the magnetic moment on the manganese coordination and nearest-neighbor distance. This result can be generalized to manganese point defects in bulk silicon. Details of the experimental setup are given elsewhere [18, 20]. Very briefly, a continuous beam of MnSi_n^+ clus-

ters is produced in a magnetron gas aggregation source and transmitted through a combined radio-frequency hexapole ion guide and collision cell into a quadrupole mass filter. After mass selection, the clusters are accumulated in a cryogenic linear Paul trap and thermalized to 10 – 20 K by collisions with helium buffer gas at $p \approx 10^{-3}$ mbar. To study the local electronic and magnetic properties of MnSi_n^+ by x-ray absorption and XMCD spectroscopy, a tunable monochromatic x-ray beam delivered by an undulator beamline at the synchrotron radiation facility BESSY II is coupled on-axis into the ion trap for resonant excitation at the manganese $L_{2,3}$ -edge. This creates Mn^+ and Si_2^+ photoions, which are detected by a reflectron time-of-flight mass spectrometer. The incident photon energy is scanned from 618 – 686 eV to record photoion yield spectra that are a measure of the x-ray absorption cross section. For XMCD spectroscopy, which requires alignment of the total magnetic moment of free MnSi_n^+ , the liquid-helium cooled ion trap is placed inside the homogeneous magnetic field ($B = 5$ T) of a superconducting solenoid, and ion yield spectra are recorded for parallel and antiparallel alignment of photon helicity and magnetic field [21]. In addition to magnetic and electronic properties, structural properties of MnSi_n^+ are investigated. Similar to the reactivity and adsorption studies of doped silicon clusters by Ohara *et al.* [22] and Janssens *et al.* [23], the exohedral-to-endohedral transition of manganese-doped silicon cluster cations is monitored via the depletion of MnSi_n^+ in the cluster beam when introducing $p \approx$

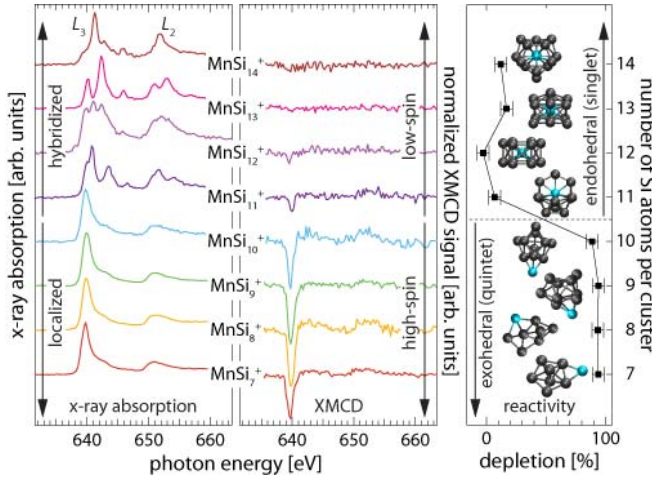


FIG. 1. (color online) Manganese $2p$ x-ray absorption (left) and XMCD (center) spectra of MnSi_n^+ clusters ($n = 7 - 14$), indicating quenched magnetic moments for $n \geq 11$; corresponding ground state structures of MnSi_n^+ and the depletion of singly doped clusters in the presence of O_2 as a measure of the exohedral-to-endohedral transition (right).

10^{-3} mbar partial pressure of oxygen reactant gas into the hexapole collision cell. As can be seen in Fig. 1, the depletion of singly doped MnSi_n^+ is 89 – 94 % for $n = 7 - 10$ but drops to 0 – 15 % for $n \geq 11$. This is due to the large difference of manganese and silicon reactivity towards oxygen that makes this depletion study a highly sensitive measure of the exohedral-to-endohedral transition, which takes place from MnSi_{10}^+ to MnSi_{11}^+ . This structural transition coincides with a marked change in the electronic properties of MnSi_n^+ as can be seen in the manganese $L_{2,3}$ x-ray absorption and XMCD spectra. These probe local $2p \rightarrow 3d$ transitions at the manganese dopant and therefore reflect its electronic structure and magnetic moment. In Fig. 1, exohedral clusters with $n = 7 - 10$ show nearly identical x-ray absorption spectra that indicate a very similar electronic structure of the manganese dopant. In contrast, the x-ray absorption spectrum and thus the local electronic structure is more complex and varies strongly with the number of silicon atoms for endohedrally doped MnSi_n^+ . Yet more striking, exohedral MnSi_n^+ shows a pronounced XMCD asymmetry that vanishes for endohedral species. Even without applying XMCD sum rules [21], the XMCD asymmetry is a qualitative and direct probe of magnetism and clearly indicates that manganese in exohedrally doped silicon clusters carries a magnetic moment which is quenched upon encapsulation. The residual XMCD asymmetry, which is observed for $n = 11$ and 12, is assigned to a slight contamination with < 5 % of $\text{Mn}_2\text{Si}_{n-2}^+$, because this XMCD signal and the corresponding lines in the x-ray absorption spectrum were tested to be proportional to the amount of $\text{Mn}_2\text{Si}_{n-2}^+$ that was observed simultaneously in mass spectrometry.

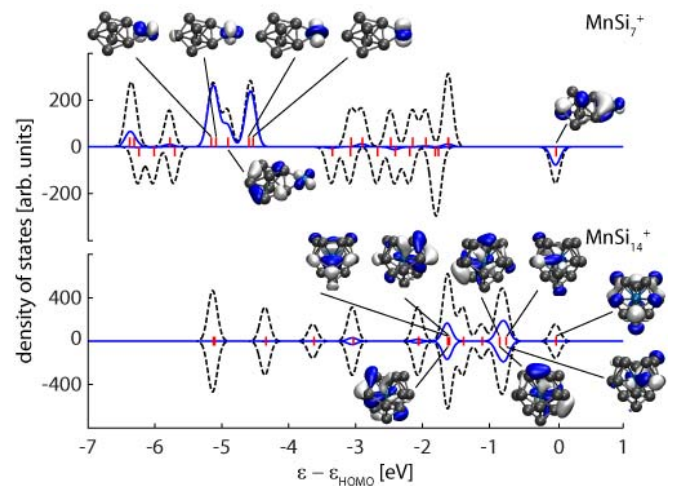


FIG. 2. (color online) Eigenvalue spectrum (bars), total (dotted line), and local Mn $3d$ -projected (solid line) DOS with isosurface plots (at ± 0.04 a.u.) of the Mn $3d$ orbitals and the highest occupied orbital for MnSi_7^+ and MnSi_{14}^+ . Positive (negative) values represent the spin-up (spin-down) channel. The d -like orbitals are localized on the manganese atom in MnSi_7^+ , whereas they are delocalized in MnSi_{14}^+ .

To further analyze the exohedral-to-endohedral and magnetic-to-nonmagnetic transition in MnSi_n^+ , we performed a thorough global geometry optimization in a simulated annealing [24] and modified “big bang” [25] approach, details of which are given in the Supplemental Material [26]. The calculations were carried out in a DFT framework using the Perdew-Burke-Ernzerhof one-parameter hybrid (PBE0) [27] as implemented in TURBOMOLE [28]. The PBE0 exchange correlation (xc) functional was chosen because it partly cancels the effects of the self-interaction error [29] that is inherent in commonly used semilocal functionals and often leads to erroneous results for the electronic structure of systems in which the highest occupied orbitals differ significantly in their degree of spatial localization [30]. This is particularly true for systems containing transition metal elements, such as MnSi_n^+ .

The assigned ground state structures of MnSi_n^+ that result from our calculations are depicted in Fig. 1. With the exception of MnSi_8^+ , the predicted structures of exohedrally doped MnSi_n^+ clusters for $n = 7 - 10$ correspond to those of Si_{n+1}^+ (cf. Refs. 19 and 31), where one silicon atom is replaced by manganese. In contrast, no structural similarity to the corresponding Si_{n+1}^+ clusters can be observed in the endohedral size regime, where manganese is encapsulated by silicon. These structural findings agree qualitatively with results of the DFT and infrared spectroscopy study by Ngan *et al.* [13]. Moreover, our calculations show that the magnetic moment of MnSi_n^+ is quenched from $4 \mu_B$ to $0 \mu_B$ at the exohedral-to-endohedral transition, in perfect agreement with the

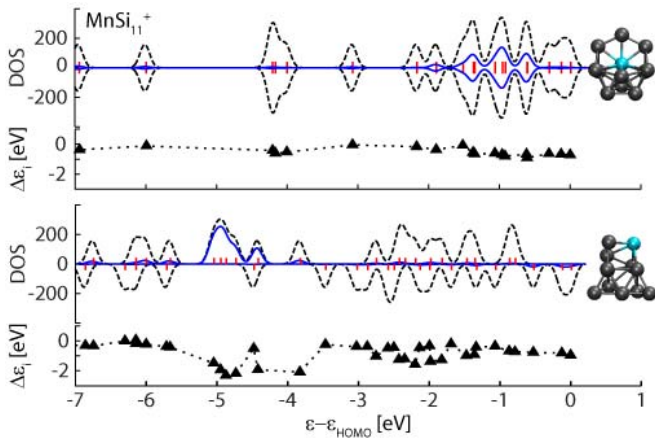


FIG. 3. (color online) Eigenvalue spectrum (bars), total DOS (dotted line), and manganese-projected local DOS (solid line) of the true endohedral ground state of MnSi_{11}^+ (top) and of the false exohedral ground state predicted by PBE0 (bottom). $\Delta\epsilon_i$ is a measure for how much the PBE0 eigenvalues are affected by the self-interaction error (see text).

experimentally observed disappearance of the XMCD signal from $n \leq 10$ to $n \geq 11$.

The change in local electronic structure of the manganese dopant that was observed in the x-ray absorption spectra at the structural transition of MnSi_n^+ in Fig. 1 is reflected in the occupied eigenvalue spectrum, which is shown in its usual interpretation as a density of states (DOS) in Fig. 2 for MnSi_7^+ and MnSi_{14}^+ , representing the exohedral and the endohedral size regime. For MnSi_7^+ , the occupied states of manganese $3d$ character are mostly isolated at $\approx 4 - 5$ eV below the Fermi level and are tightly localized at the manganese dopant, i.e., they largely preserve a (perturbed) atomic character and only weakly interact with silicon states, as can be seen from the DOS and the isosurface plots. Because of this weak interaction, the localized orbitals of manganese $3d$ character are qualitatively very similar for all exohedral MnSi_n^+ clusters and lead to the nearly identical x-ray absorption spectra in Fig. 1. This notion of, at least partly, atomic manganese $3d$ states is lost in the endohedral size regime, represented by MnSi_{14}^+ in Fig. 2. Here, orbitals with partial manganese $3d$ character are strongly hybridized with silicon states and are shifted to $\approx 0.5 - 2$ eV below the Fermi level, i.e., they participate strongly in bonding and are delocalized over the silicon frame. Consequently, the manganese $3d$ derived partial DOS sensitively depends on the structure of the silicon cage, which is reflected in the variation of the x-ray absorption spectra of endohedral MnSi_n^+ for different n in Fig. 1. As a result of strong spd hybridization with the participation of all manganese valence orbitals, the magnetic moment is completely quenched in endohedrally doped clusters. Because of the well known self-interaction error [29], a treatment of this change from a partly localized, atomic-

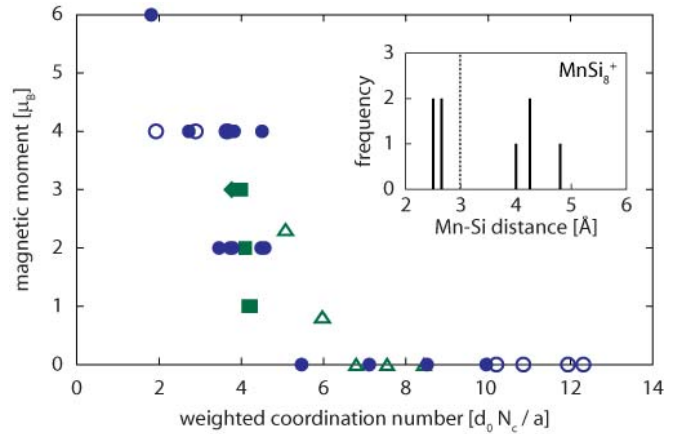


FIG. 4. (color online) Magnetic moment versus weighted coordination $d_0 N_c / a$ for ground state (open circles) and higher energy (solid circles) isomers of MnSi_n^+ ($n = 7 - 14$), isolated neutral Mn impurities in bulk ([4], solid squares) and amorphous silicon ([6], open triangles), and in a silicon nanocrystal ([8], solid diamond). Inset: bond length distribution of MnSi_8^+ with first coordination sphere (dotted line).

like situation to one in which all orbitals are delocalized on similar length scales poses serious difficulties to standard approximations of the xc functional. Therefore, the DFT results have to be analyzed carefully at the structural transition around MnSi_{11}^+ , where exohedral and endohedral isomers can be expected to be closest in energy. For MnSi_{11}^+ , PBE0 predicts an exohedral ground state with a total magnetic moment of 2 μ_B , which is 1.13 eV lower in energy than an endohedral isomer that would be in agreement with the experimental results. We attribute this discrepancy to uncertainties in theory for two reasons: First, we argue that the experimentally observed endohedral structure is indeed the ground state since we have observed ground-state structures of the related systems Si_n^+ and VSi_n^+ [16, 19, 32] under similar experimental conditions and for comparable size ranges. Second, a closer look at the theoretical result reveals that the failure of PBE0 for MnSi_{11}^+ can indeed be explained in terms of the effect of self-interaction on the eigenvalue spectrum of both isomers. The self-interaction error e_i of the orbital φ_i ,

$$e_i = \langle \varphi_i | v_H [|\varphi_i|^2] + v_{xc}^{\text{approx}} [|\varphi_i|^2, 0] | \varphi_i \rangle,$$

can be used to quantify the reliability of the eigenvalue spectrum [30]. Here v_H is the electrostatic Hartree-potential and v_{xc}^{approx} is an approximate xc potential. Details of the calculation of e_i are given in the Supplemental Material [26] and references therein [33–35]. The self-interaction corrected eigenvalues ϵ_i can be estimated as $\epsilon_i \approx \epsilon_i^{\text{approx}} - e_i$ [29], where $\epsilon_i^{\text{approx}}$ results from a self-consistent calculation using v_{xc}^{approx} . Fig. 3 compares the difference $\Delta\epsilon_i$ between ϵ_i and the PBE0 eigenvalues ϵ_i^{PBE0} as a measure of how reliably PBE0 cancels the

orbital self-interaction error in the two MnSi_{11}^+ isomers. The large value of $\Delta\varepsilon_i$ as well as its scatter shows that the exohedral PBE0 result is nonreliable in the case of MnSi_{11}^+ because self-interaction strongly affects orbitals that participate in bonding. For the endohedral isomer with delocalized orbitals, the PBE0 eigenvalues are almost identical to ε_i , and are thus reliable. In view of these arguments, we conclude that MnSi_{11}^+ is the smallest endohedral structure. This reassessment of the energetic order does not alter the observed quenching of the magnetic moment at the exohedral-to-endohedral transition since every endohedral isomer of MnSi_n^+ that resulted from our calculations is predicted to adopt a singlet state by PBE0. We therefore stress that these deliberations only lead us to reconsider the predicted critical size in accordance with our reactivity studies, but do not change the electronic or magnetic properties.

The structural change at the exohedral-to-endohedral transition of MnSi_n^+ can be quantified by the coordination number N_c of manganese, i.e., the number of silicon atoms in the first coordination sphere as exemplified for MnSi_8^+ in the inset of Fig. 4. In exohedral clusters, manganese adopts a minimal coordination number of $N_c = 2-4$, while in endohedral clusters N_c is maximized to 11–14, i.e., all silicon atoms are within the first coordination sphere of manganese. The average Mn-Si bond length a elucidates why encapsulation of the manganese dopant becomes energetically favorable only for $n \geq 11$: In the ground state structures, the Mn-Si nearest neighbor distance expands from $a = 2.43 - 2.58 \text{ \AA}$ in exohedral to $a = 2.53 - 2.67 \text{ \AA}$ in endohedral clusters. In contrast, it would be compressed to $a = 2.35 \text{ \AA}$ in the higher energy endohedral isomer of MnSi_{10}^+ . Even though manganese favors high coordination in silicon [36], this strain, which becomes even more pronounced in smaller clusters, precludes endohedral ground states for $n \leq 10$. The abrupt change in coordination at the structural transition is interrelated with the quenching of the magnetic moment as illustrated in Fig. 4: Here, the calculated magnetic moments of MnSi_n^+ are plotted versus the weighted coordination number $d_0 N_c/a$, which takes into account both the number of silicon nearest neighbors N_c as well as their average distance a to the manganese atom, normalized to the nearest neighbor distance d_0 in bulk silicon. Low-coordinated exohedral clusters with $d_0 N_c/a = 1.9-3.7$ ($N_c = 2-4$) carry a magnetic moment of $4 \mu_B$, which is quenched to $0 \mu_B$ in high-coordinated species with $d_0 N_c/a = 10.2 - 12.3$ ($N_c = 11 - 14$). This relation of magnetic moment and weighted coordination also holds for higher-energy isomers that are included in Fig. 4 and mark the transition from magnetic to nonmagnetic impurities around $d_0 N_c/a \approx 4$.

Fig. 4 shows that this observation can be generalized to extended systems, i.e., to a neutral manganese impurity at a substitutional site in crystalline silicon [4] or in hydrogen-passivated silicon nanocrystals [8]. It also

applies to very low concentrations of manganese in amorphous silicon, for which a possible relation between magnetic moment and coordination has been pointed out [6]. However, although N_c is the leading term, it does not account for the dependence of the local magnetic moment on the nearest-neighbor distance [4] that becomes important around $N_c = 4$ and is included in $d_0 N_c/a$. As can be seen in Fig. 4, manganese-doped bulk silicon is just at the transition from high-spin to low-spin states and therefore reacts very sensitively to changes in $d_0 N_c/a$. This might explain the large scatter in experimental results on manganese-doped silicon and indicates that high-spin states could be stabilized by an appropriate expansion of the lattice parameter, e.g., in ultrathin films or passivated nanocrystals.

In summary, the magnetic moment of manganese-doped silicon has been investigated over a wide range of structural parameters, including extreme coordination numbers from 2 - 14. The study of singly doped, size-selected MnSi_n^+ clusters avoids impurity-band formation or interaction between impurities that might be present in experiments on bulk samples, but also in calculations with periodic boundary conditions. We are thus able to show that the observed quenching of the magnetic moment is not a result of impurity band formation but of the electronic interaction with the silicon host. A universal correlation of the magnetic moment and the weighted coordination number is observed, providing guidelines to the stabilization of high-spin states in dilute manganese-doped silicon.

This work was supported by DFG grant No. LA 2398/5-1 within FOR 1282. Beamtime for this project was granted at BESSY II beamlines UE52-SGM and U49/2-PGM-1, operated by Helmholtz-Zentrum Berlin. The superconducting magnet was provided by Toyota Technological Institute. SK and LL acknowledge financial support by DFG SFB 840. SK additionally acknowledges support by the GIF. We thank V. Forster for providing the code for random coordinate generation, and E. Janssens for the experimental IRMPD spectra. AT acknowledges financial support by Genesis Research Institute, Inc. BvI acknowledges travel support by HZB.

* LL and VZB contributed equally to this work.

† linn.leppert@uni-bayreuth.de

‡ tobias.lau@helmholtz-berlin.de

- [1] G. W. Ludwig and H. H. Woodbury, *Solid State Phys.*, **13**, 223 (1962).
- [2] F. Beeler, O. K. Andersen, and M. Scheffler, *Phys. Rev. B*, **41**, 1603 (1990).
- [3] H. Wu, P. Kratzer, and M. Scheffler, *Phys. Rev. Lett.*, **98**, 117202 (2007).
- [4] Z. Z. Zhang, B. Partoens, K. Chang, and F. M. Peeters, *Phys. Rev. B*, **77**, 155201 (2008).

- [5] K. Sato, L. Bergqvist, J. Kudrnovsky, P. H. Dederichs, O. Eriksson, I. Turek, B. Sanyal, G. Bouzerar, H. Katayama-Yoshida, V. A. Dinh, T. Fukushima, H. Kizaki, and R. Zeller, *Rev. Mod. Phys.*, **82**, 1633 (2010).
- [6] L. Zeng, J. X. Cao, E. Helgren, J. Karel, E. Arenholz, L. Ouyang, D. J. Smith, R. Q. Wu, and F. Hellman, *Phys. Rev. B*, **82**, 165202 (2010).
- [7] X. Huang, A. Makmal, J. R. Chelikowsky, and L. Kronik, *Phys. Rev. Lett.*, **94**, 236801 (2005).
- [8] F. Küwen, R. Leitsmann, and F. Bechstedt, *Phys. Rev. B*, **80**, 045203 (2009); R. Leitsmann, C. Panse, F. Küwen, and F. Bechstedt, *ibid.*, **80**, 104412 (2009).
- [9] X. Chen, X. Pi, and D. Yang, *Appl. Phys. Lett.*, **99**, 193108 (2011).
- [10] S. N. Khanna, B. K. Rao, and P. Jena, *Phys. Rev. Lett.*, **89**, 016803 (2002).
- [11] V. Kumar and Y. Kawazoe, *Appl. Phys. Lett.*, **83**, 2677 (2003).
- [12] W. Zheng, J. M. Nilles, D. Radisic, and K. H. Bowen, Jr., *J. Chem. Phys.*, **122**, 071101 (2005).
- [13] V. T. Ngan, E. Janssens, P. Claes, J. T. Lyon, A. Fielicke, M. T. Nguyen, and P. Lievens, *Chem. Eur. J.*, **18**, 15788 (2012).
- [14] D. Palagin and K. Reuter, *Phys. Rev. B*, **86**, 045416 (2012).
- [15] J. T. Lau, J. Rittmann, V. Zamudio-Bayer, M. Vogel, K. Hirsch, P. Klar, F. Lofink, T. Möller, and B. v. Issendorff, *Phys. Rev. Lett.*, **101**, 153401 (2008).
- [16] J. T. Lau, K. Hirsch, P. Klar, A. Langenberg, F. Lofink, R. Richter, J. Rittmann, M. Vogel, V. Zamudio-Bayer, T. Möller, and B. v. Issendorff, *Phys. Rev. A*, **79**, 053201 (2009).
- [17] S. Peredkov, M. Neeb, W. Eberhardt, J. Meyer, M. Tombers, H. Kampschulte, and G. Niedner-Schatteburg, *Phys. Rev. Lett.*, **107**, 233401 (2011).
- [18] M. Niemeyer, K. Hirsch, V. Zamudio-Bayer, A. Langenberg, M. Vogel, M. Kossick, C. Ebrecht, K. Egashira, A. Terasaki, T. Möller, B. v. Issendorff, and J. T. Lau, *Phys. Rev. Lett.*, **108**, 057201 (2012).
- [19] M. Vogel, C. Kasigkeit, K. Hirsch, A. Langenberg, J. Rittmann, V. Zamudio-Bayer, A. Kulesza, R. Mitric, T. Möller, B. von Issendorff, and J. T. Lau, *Phys. Rev. B*, **85**, 195454 (2012).
- [20] K. Hirsch, J. T. Lau, P. Klar, A. Langenberg, J. Probst, J. Rittmann, M. Vogel, V. Zamudio-Bayer, T. Möller, and B. v. Issendorff, *J. Phys. B*, **42**, 154029 (2009).
- [21] B. T. Thole, P. Carra, F. Sette, and G. van der Laan, *Phys. Rev. Lett.*, **68**, 1943 (1992); P. Carra, B. T. Thole, M. Altarelli, and X. Wang, *ibid.*, **70**, 694 (1993).
- [22] M. Ohara, K. Koyasu, A. Nakajima, and K. Kaya, *Chem. Phys. Lett.*, **371**, 490 (2003).
- [23] E. Janssens, P. Gruene, G. Meijer, L. Woste, P. Lievens, and A. Fielicke, *Phys. Rev. Lett.*, **99**, 063401 (2007).
- [24] S. Kirkpatrick, C. D. Gelatt, and M. P. Vecchi, *Science*, **220**, 671 (1983).
- [25] K. A. Jackson, M. Horoi, I. Chaudhuri, T. Frauenheim, and A. A. Shvartsburg, *Phys. Rev. Lett.*, **93**, 013401 (2004).
- [26] See Supplemental Material at [URL] for details of the global optimization procedure and the calculation of the self-interaction error, as well as simulated harmonic vibrational spectra and xyz-coordinates of the MnSi_n^+ ground state structures.
- [27] C. Adamo and V. Barone, *J. Chem. Phys.*, **110**, 6158 (1999).
- [28] TURBOMOLE V6.0 2009.
- [29] J. P. Perdew and A. Zunger, *Phys. Rev. B*, **23**, 5048 (1981).
- [30] T. Körzdörfer, S. Kümmel, N. Marom, and L. Kronik, *Phys. Rev. B*, **79**, 201205(R) (2009); *Phys. Rev. B*, **82**, 129903 (2010).
- [31] J. T. Lyon, P. Gruene, A. Fielicke, G. Meijer, E. Janssens, P. Claes, and P. Lievens, *J. Am. Chem. Soc.*, **131**, 1115 (2009).
- [32] J. T. Lau, M. Vogel, A. Langenberg, K. Hirsch, J. Rittmann, V. Zamudio-Bayer, T. Möller, and B. von Issendorff, *J. Chem. Phys.*, **134**, 041102 (2011).
- [33] L. Kronik, A. Makmal, M. L. Tiago, M. M. G. Alemany, M. Jain, X. Huang, Y. Saad, and J. R. Chelikowsky, *Phys. Status Solidi B*, **243**, 1063 (2006).
- [34] J. P. Perdew, K. Burke, and M. Ernzerhof, *Phys. Rev. Lett.*, **77**, 3865 (1996).
- [35] T. Körzdörfer and S. Kümmel, *Phys. Rev. B*, **82**, 155206 (2010).
- [36] H. Wu, M. Hortamani, P. Kratzer, and M. Scheffler, *Phys. Rev. Lett.*, **92**, 237202 (2004).